Available online at www.sciencedirect.com
SCIENCE DIRECT®
Journal of Solid State Chemistry 179 (2006) 1733–1738
JOURNAL OF SOLID STATE CHEMISTRY
www.elsevier.com/locate/jssc

Self-assembly of cerium compound nanopetals via a hydrothermal process: Synthesis, formation mechanism and properties

Yuelan Zhang, Zhitao Kang, Jian Dong, Harry Abernathy, Meilin Liu*

School of Materials Science and Engineering, Georgia Institute of Technology, 771 Ferst Drive, Atlanta, GA 30332-0245, USA

Received 14 December 2005; received in revised form 7 March 2006; accepted 8 March 2006
Available online 19 April 2006

Abstract

Nanopetals of cerium hydroxycarbonate have been synthesized via a controlled hydrothermal process in a mixed water–ethanol medium. Electron microscopy indicates that each microsized flower consists of tens to hundreds of cerium hydroxycarbonate nanopetals. These nanopetals have a very large aspect ratio: a width as large as 10 μm, with a thickness as thin as 10 nm. The formation of the cerium compound depends strongly on the composition of the precursors, and is attributed to the favored ethanol oxidation by Ce(IV) ions over Ce(IV) hydrolysis process. Raman studies showed that microflower CeO_2 preferentially stabilizes O_2 as a peroxide species on its surface for CO oxidation.

Keywords: Ceria; Cerium hydroxycarbonate; Hydrothermal process; Nanopetal; Self-assembly; CO oxidation

1. Introduction

Ceria and ceria-based materials have received wide attention for various applications such as fast ion conductors (solid electrolytes as well as composite electrodes for intermediate temperature solid-oxide fuel cells) [1], catalytic supports for automotive exhaust systems and for low-cost H_2 generation in fuel cells [2], low-temperature ($<600\,^{\circ}C$) oxygen sensors and oxygen storage capacitors. The high oxygen storage capacity in conjunction with special redox properties (involving lattice oxygen/oxygen vacancy participation) can catalyze CO oxidation on the CeO_2 surface, making this system particularly useful in three-way catalysts for the treatment of automotive exhaust gas (hydrocarbons, CO and nitrogen oxides) [2c,d].

Nanostructured materials have generated a lot of interest due to their unique physical and chemical properties. This is because many properties of materials, such as catalytic activity, sensitivity or conductivity, are closely related to surface area and particle size. Preparation and controlled fabrication of ceria-based nanostructured materials with functional properties have attracted more and more attention. Masui et al. [3] have synthesized ultrafine ceria nanoparticles with diameters of 2.6 nm for CO oxidation. Mesoporous ceria has been synthesized using a templating method [4]. Cerium compound nanowires and nanorings have been obtained based on the direct-template method by AOT(bis(2-ethylhexyl) sulfosuccinate) anions and alkyl alcohols [5]. Furthermore, nanosized ceria can be synthesized from the thermal decomposition of cerium compounds, such as cerium carbonates or hydroxycarbonates [6–8]. Most previously reported work on nanostructured ceria focused on the synthesis and properties of spherical ceria nanoparticles. In this work, we report for the first time the self-assembly of a new nanostructure, microsized nanopetals of cerium compounds, by a selected hydrothermal method using a mixture of water and ethanol as a reaction medium. The effects of solvent and concentration of the precursors on the resultant phases and morphologies were investigated and discussed. A mechanism is proposed to account for the formation of the phases and the nanostructures. The catalytic properties of different nanostructures towards CO oxidation were studied using Raman spectroscopy.

*Corresponding author. Fax: +1 404 894 9140.
E-mail address: meilin.liu@mse.gatech.edu (M. Liu).

0022-4596/$ - see front matter © 2006 Elsevier Inc. All rights reserved.
doi:10.1016/j.jssc.2006.03.004

2. Experimental section

2.1. Synthesis of nanopellet cerium compound

Cerium ammonia nitrate was dissolved in distilled water. The molar ratio of water to Ce^{4+} ions ranged from 20 to 100. The solution was then added into ethanol while stirring (volumetric ratio of ethanol to water was 10:1). The resulting solution with a grape wine color was then transferred into a Teflon-lined steel autoclave and heated at 180 °C for 10 h in an electric oven. The autoclave was then quenched to room temperature. The precipitates were collected, washed by distilled water and ethanol, and dried in an oven at 80 °C. Some of the precipitates were subsequently calcined in air at 500 °C for 5 h or 800 °C for 2 h.

2.2. Characterization

The crystalline phase identification was performed through powder X-ray diffraction (XRD, PW 1800) using Cu$K\alpha$ radiation. The morphology and size of the precipitates were examined using a scanning electron microscope (SEM, LEO 1530) and a transmission electron microscope (TEM, JEOL 100C). Most samples for SEM observation were sputtered with gold, except for the one used to determine the thickness of the nanopetals. N_2 adsorption measurements were performed at 77 K with a Micromeritics ASAP 2000 system to measure specific surface area.

For the Raman spectroscopy measurements, a Renishaw RM-1000 Raman microscope was used with an Ar ion laser excitation source tuned to 488 nm. The samples were 10 mm diameter pellets that had been pressed under 1 ton from 100 mg of either nanopetal ceria powders calcined at 500 °C for 5 h or spherical ceria nanoparticles (no calcination). The pellet was then placed into a temperature- and atmosphere-controlled Raman sample chamber (special order, Harrick Scientific). The pellet was pretreated at 50 °C in vacuum (10^{-1} Pa) for 1 h before the adsorption experiment. A Raman spectrum of the pellet surface was then taken after exposure to a 10% O_2 (balance argon) atmosphere for 15 min. The pellet surface was then exposed to 10% CH_4 (balance argon) for 20 min before another spectrum was collected. Finally, the pellet was re-exposed to a 10% O_2 atmosphere. All gas flows were held at 100 ccm. Each Raman spectrum presented consists of ten 20-s spectra added together, giving a total exposure time of 200 s. The presence of any new peaks due to oxygen-containing species was confirmed using standard $^{18}O_2/^{16}O_2$ isotope exchange methods.

3. Results and discussion

3.1. Microstructures and morphologies of cerium compounds

Shown in Fig. 1 are the XRD patterns of as-synthesized cerium compound nanostructure and those obtained after calcination at 500 °C. The XRD pattern in Fig. 1a indicated that the as-synthesized cerium compound can be indexed as a mixture of hexagonal cerium carbonate hydroxide $Ce(OH)CO_3$ ($a = 7.2382$ Å and $c = 9.9596$ Å, JCPDS card No. 32-0189) with a small amount of the cubic fluorite cerium oxide ($a = 5.41134$ Å, JCPDS card No. 43-1002). The XRD spectrum from the as-synthesized sample shows a textured structure compared with the XRD spectrum acquired from the standard hexagonal cerium carbonate hydroxide powders (Fig. 1a). The strongest peaks in Fig. 1b are $\{11\bar{2}0\}$ and $\{30\bar{3}0\}$.

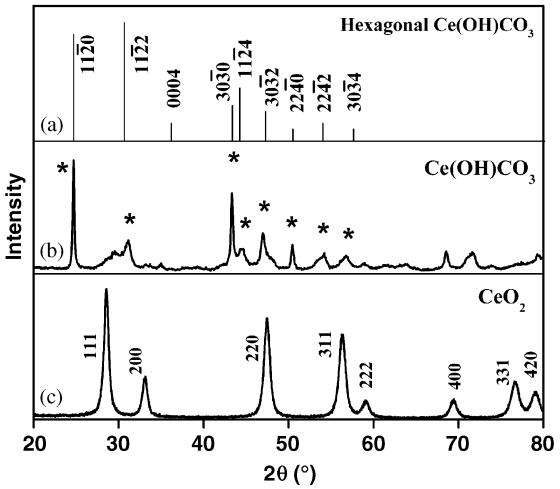

Fig. 1. (a) The standard XRD pattern of hexagonal $Ce(OH)CO_3$, (b) the as-grown cerium compounds with precursor ratio of Ce^{4+} to H_2O at 1:20, and (c) fired samples at 500 °C for 5 h.

Fig. 2 shows typical SEM images of the as-grown cerium compound with flower-like microstructures. The obtained microflowers varied in size from several microns to several tens of micrometers (Fig. 2a), and are assemblies of tens to hundreds of nanopetals (Fig. 2b). From the top view and side view of the cerium compound nanopetals, the nanopetals stack layer by layer, tending to align along some orientation, looking like blooming flowers. The nanopetals are slightly curved, several microns in width, and approximately 10 nm in thickness (Fig. 2e).

Shown in Fig. 3a–b is a TEM bright-field image of cerium compound petals and the corresponding SAED pattern. The diffraction pattern is well-indexed as [0001] zone spots with $a = 7.2382$ Å. The diffraction pattern indicates that these nanopetals have a "single crystalline" textured orientation and the side surfaces are $\{11\bar{2}0\}$ and $\{30\bar{3}0\}$ planes, in agreement with XRD results. This indicates that the growth velocity of the cerium compound nanopetal that is normal to the [0001] direction is much faster than that along the [0001] direction. The extra faded ring diffraction pattern could be indexed as ceria with cubic fluorite structure.

The specific areas for different calcination temperatures were measured. The results are 88, 97 and 36 m^2/g for the

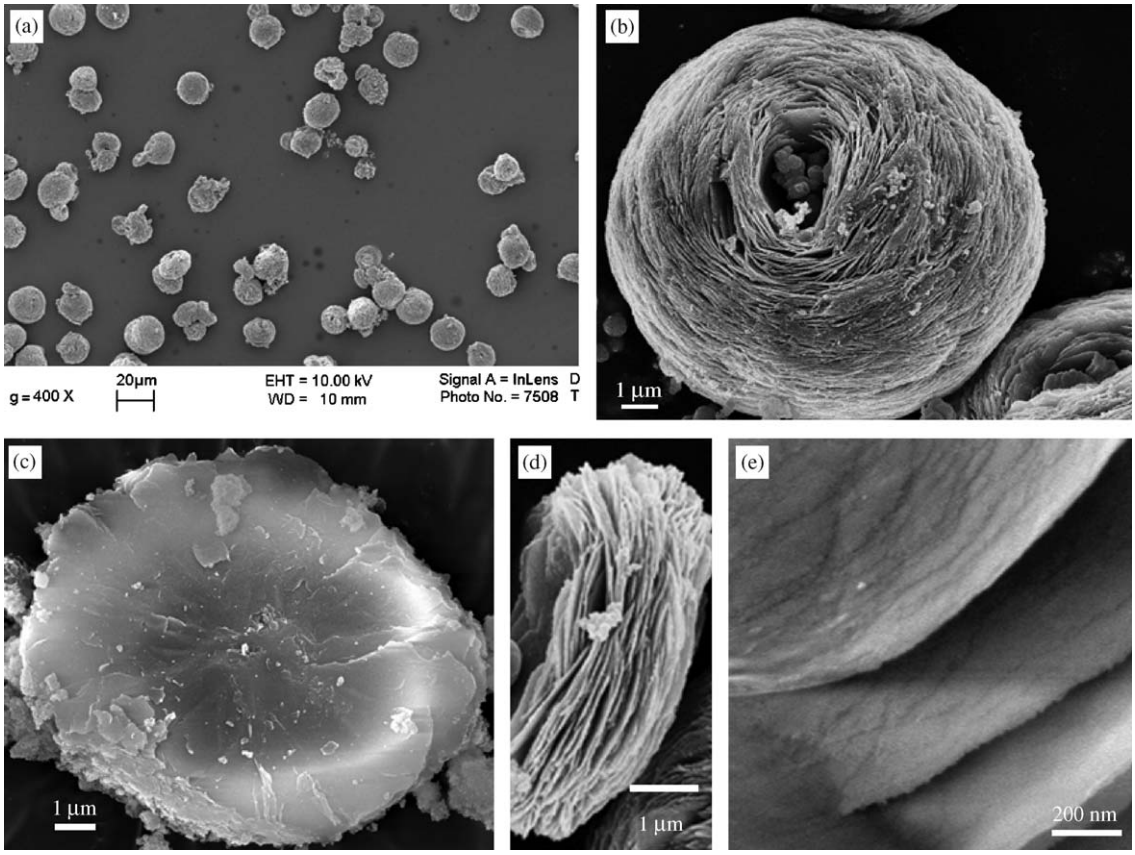

Fig. 2. SEM images of as-grown cerium compounds with microflower shape under hydrothermal conditions at 180 °C (molar ratio of Ce^{4+} to $H_2O = 1{:}20$). (a)–(b) $Ce(OH)CO_3$ microflower at different magnifications, (c) top view of nanopetals, (d) side view of the nanopetals, (e) enlarged view of nanopetals without gold coating.

as-synthesized samples, the samples calcined at 500 °C and those calcined at 800 °C, respectively. These results show the separated nanopetals were not easily sintered due to their unique structure.

3.2. Effect of ion concentration on the morphologies and phase transformation

The composition and morphology of the final product can be controlled by the cerium source, the cosolvent, and the relative concentration of metal ion and water. In this work, the precursor concentration in a mixed water–ethanol medium plays a key role in the synthesis of cerium compound nanopetals. A suitable concentration can effectively prevent hydrolysis of cerium ammonium nitrate to cerium oxide in the initial stage and kinetically control the growth of the nanostructures. When the molar ratio of water to metal ion is below 20, the product is mainly the cerium carbonate hydroxide with flower-like microstructures. However, as the ratio increases beyond 100, no nanopetals form. The obtained products were spherical aggregates of nanoparticles (Fig. 4), which were indexed to CeO_2 by XRD (Fig. 5). If the ratio was kept between 20 and 100, a combination of cerium compound microflowers and ceria nanoparticles was obtained.

3.3. Formation mechanism of nanopetal cerium compound

In this hydrothermal condition, two competing reaction processes existed: the hydrolysis of Ce^{4+} and the redox reaction between Ce^{4+} and ethanol. Both reactions are preceded by a reversible formation of a complex between Ce^{4+} and ethanol [9]. This complexation is indicated by the change of color, from a clear yellow red to a deep wine red. The chemical reaction of the oxidation of ethanol by Ce^{4+} can be formulated as

$$2Ce^{4+} + CH_3CH_2OH \rightarrow 2Ce^{3+} + CH_3CHO + 2H^+ \quad (1)$$

which comprises two half reactions

$$Ce^{4+} + e^- \rightarrow Ce^{3+}, \quad E^0 = 1.72\,V, \quad (1a)$$

$$CH_3CH_2OH \rightarrow CH_3CHO + 2H^+ + 2e^-, \quad E^0 = 0.197\,V. \quad (1b)$$

On the basis of E^0, the Gibbs free energy change of reaction (1) could be ~ -370 kJ/mol, implying a very strong

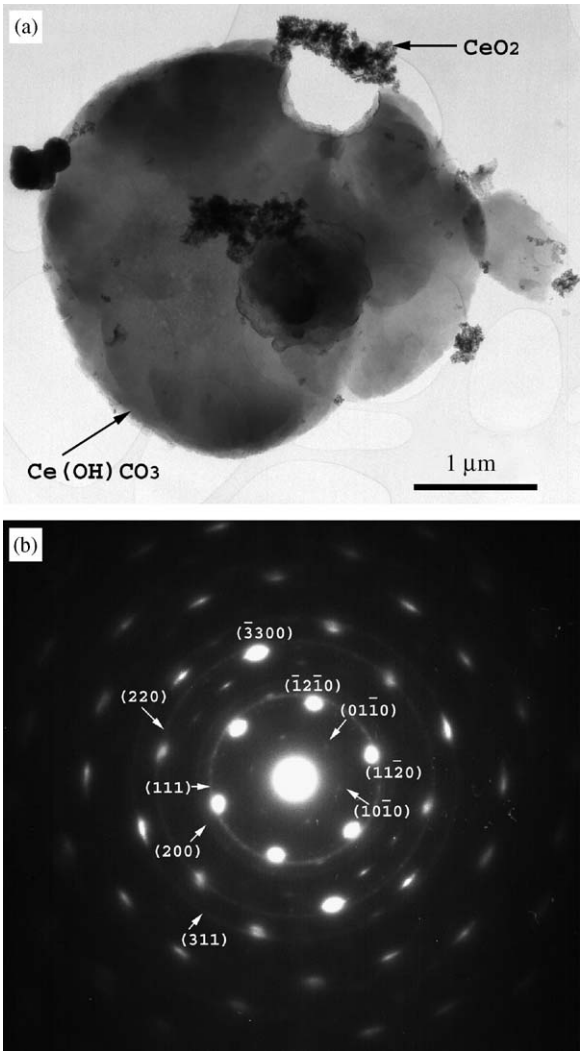

Fig. 3. (a) TEM images of cerium compound nanopetals, (b) selected-area electron diffraction (SAED) pattern of the nanopetals in (a). The spot pattern is indexed as $Ce(OH)CO_3$ nanopetals. They have textured orientation along [0001]. The shaded ring pattern is indexed as ceria.

tendency for reaction (1) to progress toward the right-hand side. The two reactions are favored energetically. It is the kinetic factors that determine which reaction would take place more favorably.

Michael Ardon [9] has investigated in detail the kinetics and mechanism of oxidation of ethanol by ceric perchlorate. The overall reaction could be described by the following steps [9]:

$$2Ce^{4+} + EtOH \Leftrightarrow \text{complex} \rightarrow 2Ce^{3+} + MeCHO + 2H^{+}. \quad (2)$$

The complex undergoes first-order decomposition into Ce^{3+} and the radical ion. This decomposition was the rate-determining step, followed by quick oxidation of the radical to acetaldehyde by a second Ce^{4+}. Then acetaldehyde could be possibly further oxidized by Ce^{4+} to acetic acid, which may decompose at elevated temperature to form CO and H_2O or (CO_2 and H_2) [10].

In the hydrothermal system, trivalent Ce^{3+} (aq) has a strong affinity with OH^- (aq). The cation will thus combine with OH^- (aq), forming the $Ce(OH)^{2+}$ (aq) polyatomic group [11]. At elevated temperatures, CO_3^{2-} will bond with the positive-charged groups to yield the solid $Ce(OH)CO_3$ at high supersaturation. The nascent crystallites act as seeds for succeeding crystal growth. When the concentration of the ceric ion decreased to some extent, the hydrolysis of Ce^{4+} overwhelmed the reduction of Ce^{4+}, so that a small amount of ceria was precipitated out. Hence, by changing the metal ion-to-water ratio, the relative rates of hydrolysis of Ce^{4+} and reduction of Ce^{4+} by ethanol could be controlled.

Regarding the growth process, although it is still not clear why the nanopetals self-assemble into the resulting flower-like microstructures, we think in the present study the growth of nanopetals favored by {0001} faces is possibly governed by crystal structure, surface energy and driving force. The {0001} face is a close-packed face of the lowest surface energy in hexagonal system. It is the general principle in forming a self-assembled nanostructure to maximize the packing density. The two-dimensional nucleation growth is possibly because higher supersaturation at the edges is expected than the central area under hydrothermal condition [12], and higher topological defect density is expected at the edge, both of which favor radial growth.

3.4. Surface properties of the different CeO_2 morphologies

Raman spectroscopy was used to characterize the oxygen species formed on nanopetal CeO_2 surface. The surface oxygen species were proven by switching 10% $^{16}O_2$ (balance Ar) to 10% $^{18}O_2$ (95% $^{18}O_2$/5% $^{16}O_2$, balance Ar). The Raman spectrum in Fig. 6 shows bands at 831 cm^{-1} which are assigned to the adsorption of η^2 peroxide species [13,14]. Former studies revealed that CO could interact with species characterized by vibrational bands at 831 cm^{-1} [13]. In this work, CH_4 was used to study the oxidation reactivity of the adsorbed species. The band at 831 cm^{-1} disappeared after exposure to CH_4 for 20 min (Fig. 6c) and then re-appeared when exposed to O_2 atmosphere again (Fig. 6d). The result indicated that the absorption and removal of surface species is reversible.

Fig. 7 compares the Raman spectrum of the ceria microflowers sintered at 500 °C to that of spherical ceria nanoparticles. The ceria samples had been reduced in 5% H_2 at 400 °C and then were exposed to 10% O_2 (balance argon) at room temperature. Both morphologies demonstrate the 831 cm^{-1} peak which has been previously assigned to an adsorbed peroxide species [13]. The 1128 cm^{-1} peak observed from the nanoparticles sample has been attributed to a surface superoxide

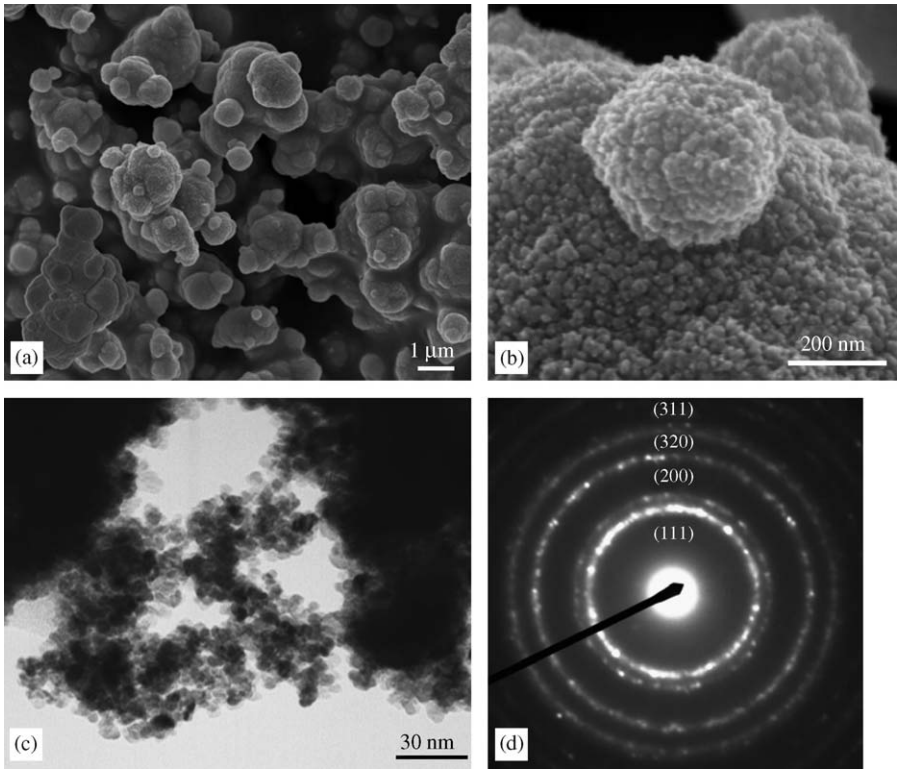

Fig. 4. (a,b) SEM images of as-prepared ceria; (c) TEM image of as-prepared ceria in (a) and (b); (d) SAED pattern of as-prepared ceria in (c). The molar ratio of Ce^{4+} to H_2O is 1:100.

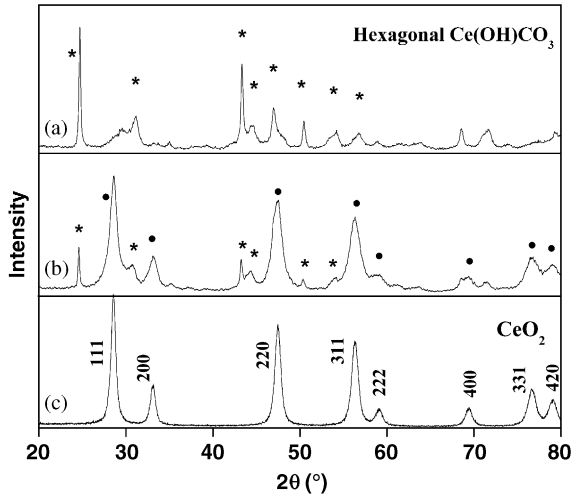

Fig. 5. XRD patterns of the as-grown cerium compounds with the precursor ratio of Ce^{4+} to H_2O at (a) 1:20, (b) 1:40, (c) 1:100. (* stands for hexagonal $Ce(OH)CO_3$, and filled circles stand for CeO_2.)

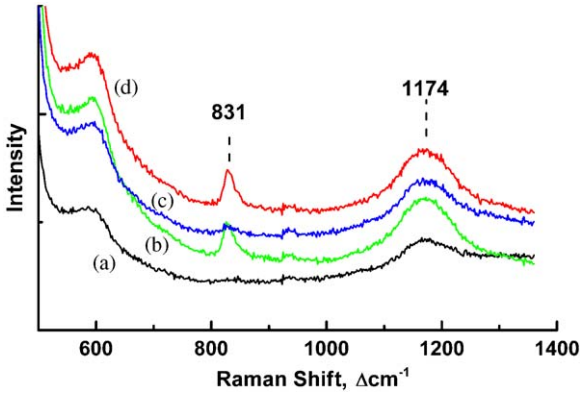

Fig. 6. Raman spectra of a CeO_2 microflower sample collected (after evacuation at 50 °C) at room temperature sequentially in (a) Ar, (b) 10% O_2 + Ar, (c) 10% CH_4 + Ar and (d) 10% O_2 + Ar.

species and, unlike the 831 cm^{-1} species, has been shown to be directly involved with CO oxidation [14]. Since the intensity of 1128 cm^{-1} peak is much weaker for the microflower sample than for the nanoparticles, the microflower ceria with its different morphology probably exhibits different catalytic activities towards CO oxidation.

In summary, we have synthesized a unique cerium compound nanostructure via a controlled hydrothermal process. The nanopetals are ~10 μm in diameter and ~10 nm in thickness. This nanostructure retains high surface area at high temperature due to the unique structure. Raman results indicated that nanopetal CeO_2 stabilizes O_2 predominantly as a peroxide species on its surface. The bare site for η^2 peroxide species is easily formed and destroyed. The CeO_2 nanopaticles stabilize O_2 as both peroxide and superoxide species.

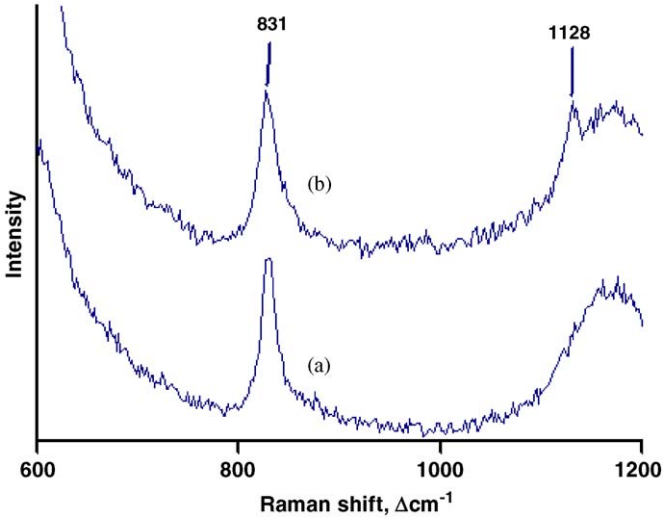

Fig. 7. Raman spectra characterizing O_2 adsorption (a) on CeO_2 microflowers with aggregated nanoparticles and (b) on CeO_2 nanoparticles, both of which had been exposed to 5% H_2 at 400 °C and then exposed to 10% O_2.

Acknowledgment

One of the authors thank Zhen Zhou and Dr. Shaowu Zha for their helpful technical discussion and Zhe Cheng for technical assistance. This work was supported by DOE-NETL under Grant No. DE-FC26-02NT41572.

References

[1] (a) T. Hibino, A. Hashimoto, T. Inoue, J. Tokuno, S. Yoshida, M. Sano, Science 288 (2000) 2031;
(b) Y. Liu, S. Zha, M. Liu, Adv. Mater. 16 (2004) 256.

[2] (a) G.A. Deluga, J.R. Salge, L.D. Schmidt, X.E. Verykios, Science 303 (2004) 993;
(b) J.P. Breen, R. Burch, H.M. Coleman, Appl. Catal. B 39 (2002) 65;
(c) J.A. Zarur, J.Y. Ying, Nature 403 (2000) 65;
(d) S. Carrettin, P. Concepcion, A. Corma, J.M.L. Nieto, V.F. Puntes, Angew. Chen. Int. Ed. 43 (2004) 2538.

[3] T. Masui, K. Fujiwara, K. Machida, G. Adachi, T. Sakata, H. Mori, Chem. Mater. 9 (1997) 2197.

[4] D.M. Lyons, K.M. Ryan, M.A. Morris, J. Mater. Chem. 12 (2002) 1207.

[5] M. Yada, S. Sakai, T. Torikai, T. Watari, S. Furuta, H. Katsuki, Adv. Mater. 16 (2004) 1222.

[6] M. Hirano, E. Kato, J. Mater. Sci. Lett. 18 (1999) 403.

[7] R.J. Qi, Y.J. Zhu, G.F. Cheng, Y.H. Huang, Nanotechnology 16 (2005) 2502.

[8] H.C. Wang, C.H. Lu, Mater. Res. Bull. 37 (2002) 783.

[9] M. Ardon, J. Chem. Soc. (1957) 1811.

[10] (a) B. Basavalingu, J. Tareen, T.N. Kutty, in: S. Somiya (Ed.), Proceedings of the First International Symposium on Hydrothermal Reactions, 1982, Gakujutsu Bunken Fukyu-Kai, Ookayama, Meguru, 1983, p. 738;
(b) M.N. Viswanathiah, J.A. Tareen, T.R.N. Kutty, in: S. Somiya (Ed.), Proceedings of the First International Symposium on Hydrothermal Reactions, 1982, Gakujutsu Bunken Fukyu-Kai, Ookayama, Meguru, 1983, p. 747.

[11] Z.H. Han, Y. Qian, S. Yu, K. Tang, H. Zhao, N. Guo, Inorg. Chem. 39 (2000) 4380.

[12] I. Sunagawa, Investigations of crystal growth in earth and planetary sciences, in: D.T.J. Hurle (Ed.), Bulk Crystal Growth, 2a Basic Techniques, North-Holland, Amsterdam, 1993.

[13] V.V. Pushkarev, V. Kovalchuk, J. d'Itri, J. Phys. Chem. B 108 (2004) 5341.

[14] J. Guzman, S. Carrettin, A. Corma, J. Am. Chem. Soc. 127 (2005) 3286.